OPEN ACCESS

ACTA METALLURGICA SLOVACA

2026, VOL. 32, NO. 3, 256-261

RESEARCH PAPER

Investigation of the properties of shell molds for investment casting quasi-high-entropy alloys

Svetlana Kvon[1], Aizhan Abildina[1], Vitaliy Kulikov[1]*

[1]Department of Metallurgy and Advanced Materials, Karaganda Technical University named after Abylkas Saginov, 56 Nursultan Nazarbayev Avenue, Karaganda, Kazakhstan; svetlana.1311@mail.ru, aizhan--1984@mail.ru, mlpikm@mail.ru

*Corresponding author: aizhan--1984@mail.ru, Department of Metallurgy and New Materials, Karaganda Technical University named after Abylkas Saginov, Karaganda, Kazakhstan

Received: 03.08.2026
Accepted: 24.08.2026

ABSTRACT

The performance of ceramic shell molds for investment casting prepared using fused quartz was evaluated. The quartz raw material was obtained from the Aktas deposit in Kazakhstan. The developed shell molds were intended for the precision casting of high-alloy materials. Fused quartz was produced by melting natural quartz at 1750 °C, followed by rapid cooling to obtain an amorphous structure. X-ray diffraction (XRD) analysis confirmed the absence of crystalline SiO_2 phases and revealed a broad diffuse halo characteristic of amorphous silica. The ceramic slurry was prepared using fused quartz as the refractory filler and 15A silica sol as the inorganic binder. The ceramic shell molds were fabricated using a five-layer dipping process with controlled intermediate drying, followed by firing at 800 °C. The developed shell molds exhibited a high gas permeability of 143 conventional units, exceeding that of the reference shell system based on quartz sand. The residual compressive strength reached 35.75 ± 1.10 MPa, indicating sufficient mechanical integrity during molten metal pouring. Experimental casting of a Fe–Cr–Mn–Co–Ni–Nb–Mo alloy revealed no visible evidence of significant mold–metal interaction, burn-on, metal penetration, or other macroscopic surface defects under the investigated casting conditions. The ceramic shell molds maintained their structural integrity during pouring and cooling, demonstrating satisfactory performance for high-temperature investment casting.

Keywords: shell molds; investment casting; fused quartz; high-alloy materials; compressive strength; gas permeability

INTRODUCTION

Investment casting is a well-established manufacturing process for producing castings with complex geometries, high dimensional accuracy, and excellent surface quality [1-3]. Because it can manufacture near-net-shape components with minimal machining allowances, this technology is widely used in the aerospace, power generation, automotive, and general engineering industries to produce components from heat-resistant and high-alloy materials.

In recent years, considerable attention has focused on quasi-high-entropy alloys (QHEAs) because they can combine high mechanical strength, wear resistance, heat resistance, and thermal stability, making them promising structural materials for applications under severe mechanical and thermal loading conditions [4-6]. However, the casting of QHEAs remains technologically challenging. Owing to their complex multicomponent compositions, these alloys may exhibit a relatively wide liquidus–solidus temperature interval, which can complicate melt processing and solidification. In addition, multiple alloying elements can result in high hardness and strength, which may make post-casting machining difficult and economically undesirable. Consequently, investment casting is considered a suitable manufacturing route for producing near-net-shape components from QHEAs.

Previous studies of heat-resistant Ni–Cr-based alloys have demonstrated the importance of alloy composition and alloying additions in controlling high-temperature strength and heat resistance. In particular, researchers have investigated how alloying elements and chemical composition affect the heat resistance and durability of Ni–Cr alloys [7, 8]. These studies highlight the importance of selecting appropriate alloy compositions and processing conditions for high-temperature applications of complex alloy systems.

The pouring temperature of QHEAs generally exceeds 1600 °C [2]. Therefore, ceramic shell molds intended for casting these alloys must possess high mechanical strength, dimensional stability, gas permeability, and chemical inertness at elevated temperatures. Insufficient mechanical strength, dimensional stability, gas permeability, or chemical inertness may result in shell cracking, metal penetration, gas porosity, and other casting defects that adversely affect the quality and reliability of the final castings [3, 9].

Conventional ceramic shell molds are typically produced using silica-based refractory materials containing crystalline quartz [2, 10, 11]. However, crystalline quartz exhibits several inherent limitations. During heating, it undergoes polymorphic phase transformations accompanied by changes in crystal structure, specific volume, and thermophysical properties. These transformations can generate internal stresses that reduce shell strength, impair dimensional stability, and increase ceramic shells' susceptibility to cracking during casting [10, 11].

To overcome these limitations, considerable research has focused on developing fused-quartz-based ceramic shell materials for high-temperature investment casting [10-12]. Because of its amorphous structure, fused quartz has a very low coefficient of thermal expansion, high thermal shock resistance, and good dimensional stability at elevated temperatures [5, 9]. When combined with silica sol as an inorganic binder, fused quartz enables the fabrication of ceramic shell molds with a relatively homogeneous microstructure, high chemical purity, and improved thermal and mechanical performance [11, 12].

Previous studies have demonstrated that replacing crystalline quartz with fused quartz can reduce thermal stresses within ceramic shells, improve dimensional stability, and decrease the likelihood of crack formation during mold fabrication and casting [5, 9]. At the same time, the performance of ceramic shell molds depends not only on the chemical composition of the refractory filler but also on particle morphology, pore structure, and interfacial interactions between the refractory filler and the binder system [12, 13].

Despite the substantial body of research devoted to fused-quartz ceramic shell systems, their application to high-temperature investment casting has received limited attention in the Republic of Kazakhstan. Several studies conducted in Kazakhstan have addressed the development of refractory materials and binder systems for investment casting, including fused-quartz-based shell molds for the precision casting of complex alloys [14, 15]. However, the application of fused-quartz ceramic shell systems specifically for high-temperature investment casting of QHEAs has not yet been sufficiently investigated in the Republic of Kazakhstan, and systematic data on the performance of shells produced from domestic quartz raw materials remain limited. Consequently, conventional silica-based refractory materials may still be widely used in domestic investment casting applications, which can limit the quality and reliability of castings produced under high-temperature conditions.

At the same time, Kazakhstan possesses high-purity quartz deposits, including the Aktas deposit in the Ulytau Region, containing more than 99 wt.% SiO_2 and only minor concentrations of impurity oxides. These characteristics indicate its potential as a domestic raw material source for fused-quartz production. Using locally available quartz raw materials may help develop a domestic refractory-material base and reduce dependence on imported materials.

Although previous studies have established the advantages of fused quartz for investment casting, the combined performance of gas permeability, residual compressive strength, coefficient of linear thermal expansion, and casting surface quality of shell molds produced using fused quartz derived from the Aktas deposit has not been sufficiently investigated under conditions relevant to QHEA casting. In particular, the relationship between the refractory filler, binder system, shell properties, and casting quality requires further experimental evaluation.
Therefore, the objective of the present study was to investigate the properties of ceramic shell molds manufactured using fused quartz produced from quartz raw material obtained from the Aktas deposit and to evaluate their performance during the investment casting of a Fe–Cr–Mn–Co–Ni–Nb–Mo QHEA. Particular attention was given to gas permeability, residual compressive strength, coefficient of linear thermal expansion, and the surface quality of the resulting castings.

MATERIAL AND METHODS

Fused quartz produced from natural vein quartz obtained from the Aktas deposit was used as the silica-based refractory filler. A commercial 15A silica sol containing 30 wt.% SiO_2 was used as the inorganic binder.
The fused quartz was produced by melting quartz particles measuring 5-10 mm in a graphite crucible using a UIP-10 laboratory induction furnace under an inert atmosphere. The quartz was heated to 1750 °C and held for 15 min to ensure complete melting. To prevent carbon contamination of the melt, the inner surface of the graphite crucible was coated with a ZKP-200 boron nitride-based protective slurry. After complete melting, the material was rapidly cooled to promote amorphous structure formation. The resulting fused quartz was then crushed and sieved to obtain a particle-size fraction of 0.2-0.6 mm.
The fabrication of ceramic shell molds comprised the following stages: preparation of wax patterns, preparation of the ceramic slurry, formation of multilayer ceramic shells, dewaxing, and high-temperature firing. Wax patterns were produced using silicone molds and a wax composition consisting of 65 wt.% paraffin, 25 wt.% microcrystalline wax, and 10 wt.% stearin. The wax mixture was melted at 75–80 °C and subsequently cast into silicone molds. After removal from the molds, the patterns were cleaned and degreased with ethanol to improve the adhesion of the primary ceramic coating. The ceramic slurry was prepared by mechanical mixing for 15 min. Its composition was as follows (wt.%): 70 wt.% fused quartz, 25 wt.% 15A silica sol, and 5 wt.% distilled water. The dynamic viscosity of the slurry was monitored using an A&D SV-1A vibrational viscometer and averaged 43.2 mPa·s. The primary ceramic layer was deposited by dip coating and subsequently stuccoed with fused quartz particles having a grain size of 0.2 mm. Each layer was dried at 20-25 °C and a relative humidity of 40-60% for 4-6 h. Four subsequent backup layers were produced using the same procedure; however, fused quartz particles measuring 0.3-0.6 mm were used as the stucco material. Thus, a five-layer ceramic shell mold was obtained.
The wax patterns were removed by gradual heating to 120 °C. The ceramic shell molds were subsequently fired in a laboratory SNOL muffle furnace (Lithuania) at 800 °C for 1-2 h **(Fig. 1a).**
To evaluate the casting performance of the developed ceramic shell molds, experimental castings were produced from a Fe–Cr–Mn–Co–Ni–Nb–Mo QHEA with the following chemical composition (wt.%): Co 15.86, Cr 15.92, Fe 17.35, Ni 15.60, Mn 16.30, Nb 14.43, C 0.40, and Mo 4.12. The alloy was melted in a UIP-10 laboratory induction melting furnace **(Fig. 1b).**
The melt temperature was monitored using an optical pyrometer. Before pouring, the ceramic shell molds were preheated to 900 °C. Casting was performed under gravity at a melt temperature of 1600 °C.
The surface morphology and microstructure of the fused quartz particles were characterized using a JEOL JCM-7000 NeoScope scanning electron microscope (SEM, Japan) operated at an accelerating voltage of 5 kV. The elemental composition was determined by energy-dispersive X-ray spectroscopy (EDS), and the spatial distribution of the constituent elements was examined by elemental mapping. The acquisition time for each EDS spectrum was 30 s.

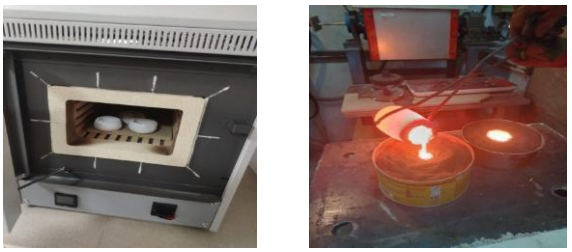

a **b**

Fig. 1 Ceramic shell molds: (a) fired ceramic shell mold before casting; (b) pouring of the molten alloy into the ceramic shell mold

To further assess the possibility of interaction between the ceramic shell and the molten alloy during casting, the surface of the experimental casting was examined by micro-X-ray spectral analysis using EDS at different locations that had been in contact with the ceramic shell. The analysis included examination of the surface microstructure at different magnifications, elemental distribution mapping, and EDS spectral analysis.
The gas permeability of the fired ceramic shell molds was determined using a Model 04315M permeability tester in accordance with GOST 23409.6-78 [16]. The test method was based on measuring the time required for a specified volume of air to pass through the specimen under a constant pressure differential. Measurements were performed in triplicate, and the reported values represent the mean of the repeated measurements. According to the instrument documentation, the measurement error did not exceed 0.5%.
The residual compressive strength of the fired ceramic shell molds was measured using an Instron 5982 universal testing machine (Instron, USA). The crosshead speed was maintained at 1 mm min^{-1}. Three specimens were tested, and the results are presented as the mean value ± standard deviation [17].
The coefficient of linear thermal expansion (CLTE) was determined using a DIL 402 push-rod dilatometer. Measurements were performed in air at a heating rate of 1 °C min^{-1} up to a maximum temperature of 1200 °C. Changes in specimen length were continuously recorded using a high-sensitivity linear variable differential transformer (LVDT) displacement sensor. Measurements were performed in triplicate, and the reported values represent the mean of the repeated measurements. According to the instrument documentation, the measurement error did not exceed 0.5%.
The surface roughness of the experimental castings was evaluated using a portable TIME TR220 surface profilometer. Surface profilometry was performed at three locations on each casting surface using a 2.5 mm cut-off length. For each measurement, the arithmetic mean surface roughness (Ra) was determined automatically, and the final Ra value was calculated as the average of the three measurements.

RESULTS AND DISCUSSION

X-ray diffraction (XRD) analysis of the fused quartz produced from natural quartz of the Aktas deposit confirmed its predominantly amorphous structure. As shown in Fig. 2, the diffraction pattern is characterized by a broad diffuse halo in the range of approximately 20-30°, while no distinct diffraction peaks are observed at 20.8°, 26.6°, and 50.1°, which are characteristic reflections of crystalline quartz (SiO_2). These results indicate that no detectable crystalline silica phases were present within the detection limits of the XRD analysis, confirming the successful transformation of crystalline quartz into an amorphous fused-quartz structure during melting followed by rapid cooling.

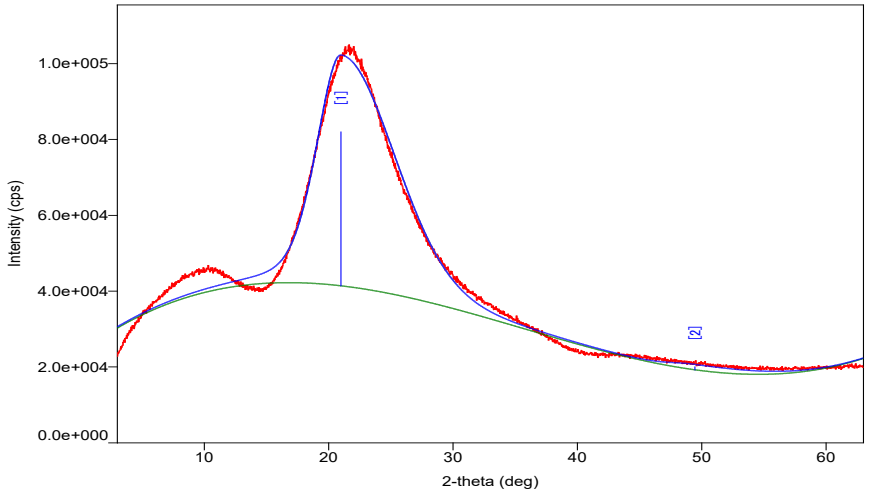

Fig. 2 X-ray diffraction (XRD) pattern of fused quartz from the Aktas deposit

The XRD results indicate that the material is predominantly amorphous after melting and rapid cooling. The absence of long-range atomic order eliminates the polymorphic transformations characteristic of crystalline quartz during subsequent heating. This structural feature is associated with the high thermal stability of fused quartz at elevated temperatures.

SEM observations **(Fig. 3a)** revealed that the fused quartz particles exhibit an angular morphology with a well-developed surface microrelief. Such morphological characteristics may increase the effective contact area between the refractory filler and the silica sol binder, potentially contributing to improved interparticle bonding during firing. In addition, the particles exhibited a relatively homogeneous microstructure without visible cracks or other surface defects, suggesting the absence of significant structural defects in the examined fused quartz particles produced from the Aktas quartz raw material.

Elemental mapping **(Fig. 3b)** further confirmed the relatively homogeneous distribution of the principal constituent elements, silicon (Si) and oxygen (O), throughout the examined particles. No pronounced elemental segregation or localized compositional inhomogeneity was observed, indicating a relatively uniform elemental distribution within the analyzed areas of the fused quartz.

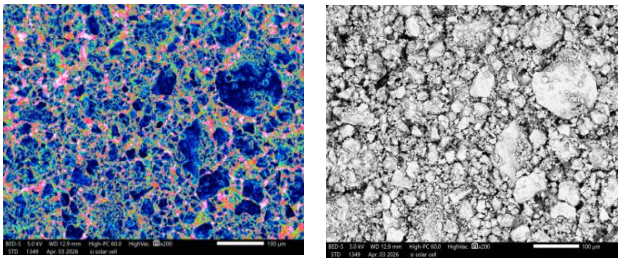

a **b**

Fig. 3 SEM images of the fused quartz: (a) particle morphology and distribution; (b) elemental mapping of the principal constituent elements (×200)

The results of the quantitative local EDS analysis **(Fig. 4)** confirmed the presence of the principal constituent elements of the refractory filler. The complete elemental composition of the fused quartz, together with the corresponding analytical parameters, is presented in **Table 1.**

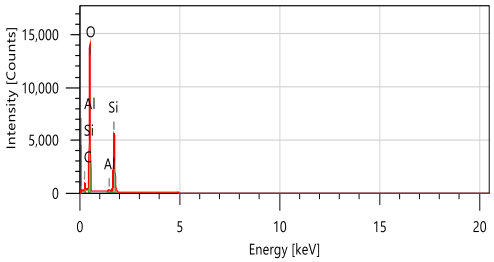

Fig. 4 EDS spectrum and analytical parameters of the elemental composition of the fused quartz

Table 1 Results of the EDS Elemental Analysis of the Fused Quartz

Element	*Weight (wt.%)*	*Atomic (at.%)*
C	6.55±0.04	10.91±0.07
O	41.75±0.12	52.22±0.15
Al	0.73±0.05	0.54±0.04
Si	50.98±0.30	36.33±0.21
Total	100.00	100.00

A minor amount of aluminum (0.73 wt.%) was also detected and found to be relatively uniformly distributed within the analyzed areas. The presence of aluminum may be associated with minor impurities in the raw material or with processing-related contamination.

A carbon content of 6.55 wt.% was detected as a result of the conductive carbon coating applied prior to SEM examination to minimize specimen charging during electron microscopy. Therefore, the detected carbon was not considered an intrinsic constituent of the fused quartz.

The fired ceramic shell molds were subsequently characterized in terms of gas permeability, residual compressive strength, and coefficient of linear thermal expansion (CLTE).

Fig. 5 presents a representative compressive stress-displacement curve obtained for the fused-quartz ceramic shell mold during the compression test.

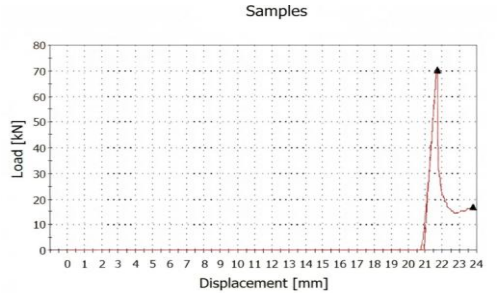

Fig. 5. Compressive stress–displacement curve of the fused-quartz ceramic shell mold.

The stress-displacement curve exhibits characteristic brittle fracture behavior, with an approximately linear increase in stress up to the maximum stress, followed by a sharp decrease in load-bearing capacity after reaching the peak stress. This behavior is consistent with the brittle fracture characteristics commonly observed in ceramic materials, in which crack initiation and rapid crack propagation occur with limited plastic deformation.

The measured gas permeability, residual compressive strength, and coefficient of linear thermal expansion of the developed ceramic shell molds are summarized in **Table 2.** For comparison, corresponding data for ceramic shell molds based on quartz sand are also included.

Table 2 Comparison of the Performance Characteristics of Ceramic Shell Molds

Material	***Gas Permeability (conventional units)***	***Residual Compressive Strength (MPa)***	***Coefficient of Linear Thermal Expansion (×10⁻⁶ K⁻¹)***
Quartz sand	60-90	27.5	12.67
Fused quartz (Aktas)	143	35.75±1.10	0.8

As shown in **Table 2**, the ceramic shell molds fabricated from fused quartz exhibited higher gas permeability than the reference quartz-sand shell system. Gas permeability is strongly influenced by pore structure, including pore size, morphology, and spatial distribution. Previous studies have shown that these parameters, along with the mechanisms governing pore-structure formation, can significantly affect the functional properties of porous materials [18-20]. In ceramic shell molds, gas transport is also affected by the packing of refractory particles and the characteristics of the binder system [12, 13, 21].

In the present shell system, the measured gas permeability may therefore be associated with the packing characteristics of the fused-quartz particles and the silica-sol binder system. The amorphous structure of fused quartz may also contribute to dimensional stability during heating by eliminating the polymorphic transformations characteristic of crystalline quartz. However, because the present study did not directly quantify open porosity, pore-size distribution, or pore morphology, the specific contribution of these parameters to the measured gas permeability cannot be established conclusively.

The developed ceramic shell molds exhibited a residual compressive strength of 35.75 ± 1.10 MPa, which was higher than that of the reference quartz-sand shell system. Notably, the increase in gas permeability was not accompanied by a reduction in mechanical strength, indicating that the enhanced gas transport was achieved without compromising the measured mechanical integrity of the shell. This combination of properties is particularly important for investment casting, where efficient gas evacuation and sufficient mechanical strength of the ceramic shell mold are required during mold filling and solidification.

After complete cooling, the casting was removed from the ceramic shell mold, followed by visual examination of both the mold and the casting **(Fig. 6).** The ceramic shell mold was readily separated from the casting, and no significant adhesion between the casting and the ceramic shell was observed. The shell retained its structural integrity after casting, with no visible cracks or delamination. The surface of the experimental casting was free from visible burn-on, and no visible metal penetration or other macroscopic surface defects were observed **(Fig. 6b).**

a **b**

Fig. 6 Experimental specimens after casting: (a) ceramic shell mold containing the casting after solidification; (b) experimental casting after removal of the ceramic shell mold

As shown in **Fig. 6a**, the ceramic shell mold retained its structural integrity throughout the casting process. Following molten metal pouring and complete cooling, no cracks, delamination, or other visible damage were observed. This result is consistent with previous findings indicating that structural homogeneity of the mold material is a key factor governing crack resistance of ceramic shells during casting [22]. These observations indicate sufficient structural stability of the ceramic shell under the investigated casting conditions.

The surface of the experimental casting **(Fig. 6b)** was free from visible surface defects, including burn-on, metal penetration, and adhesion of ceramic shell material to the casting. These observations indicate no evidence of significant macroscopic interaction between the ceramic shell and the molten alloy under the investigated casting conditions.

The relatively high gas permeability of the shell mold provided favorable conditions for gas evacuation during mold filling and alloy solidification. However, the present study did not directly quantify the specific contribution of pore structure to gas transport.

To further assess the possibility of interaction between the ceramic shell and the molten alloy during casting, the present study examined the experimental casting surface by micro-X-ray spectral analysis using EDS at different locations on the casting surface that had been in contact with the ceramic shell. The analysis included examination of the surface microstructure at different magnifications, elemental distribution mapping, and EDS spectral analysis.

As shown in **Fig. 7,** the EDS spectra obtained from the analyzed locations on the casting surface did not reveal a detectable Si signal.

The detected elemental composition consisted mainly of the alloying elements Fe, Cr, Mn, Co, Ni, Nb, and Mo, together with carbon. Since silicon is the principal constituent of the ceramic shell, the absence of a detectable Si signal in the analyzed spectra indicates that no measurable transfer of silicon from the ceramic shell to the casting surface occurred under the investigated casting conditions. These results provide additional evidence of the chemical compatibility of the developed fused-quartz ceramic shell with the investigated alloy under the applied casting conditions.

The average surface roughness of the experimental casting was Ra = 2.65 μm, corresponding to surface roughness grades 5-7 according to the applicable surface roughness classification.

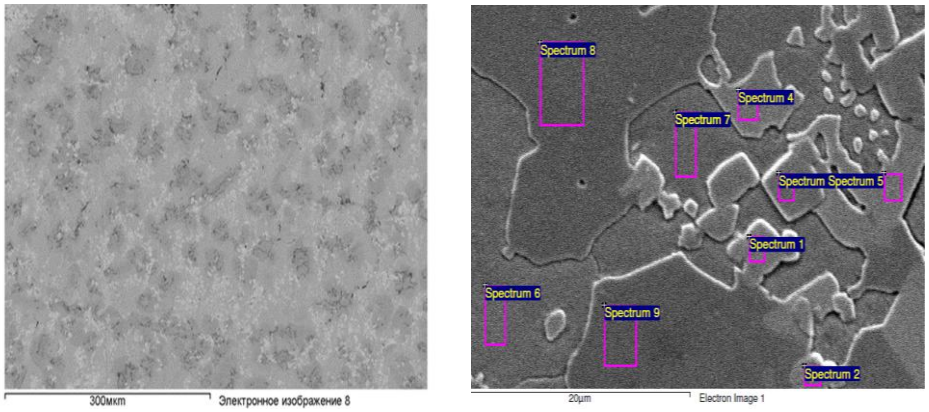

a

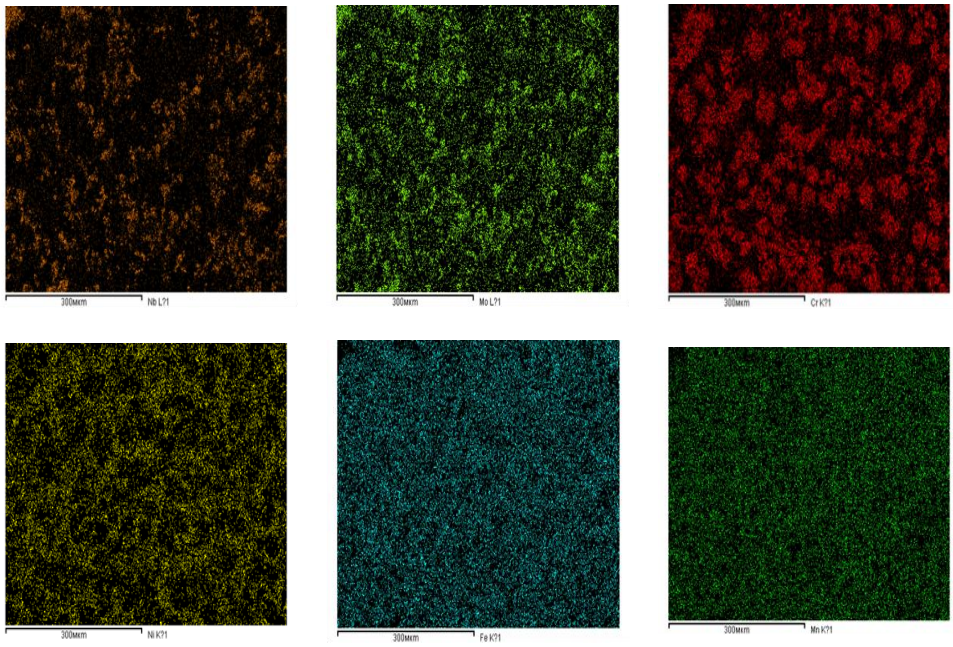

b

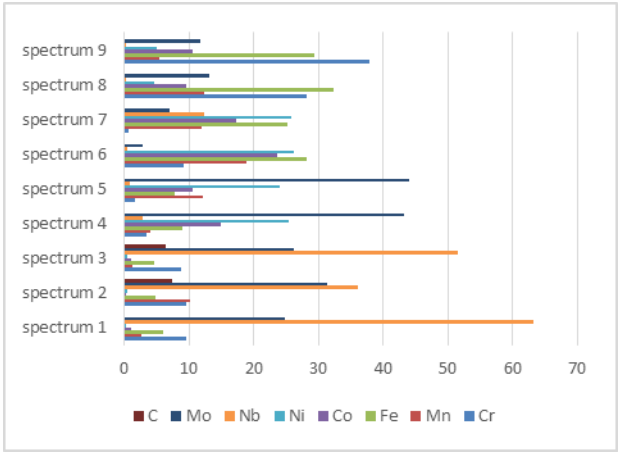

c

Fig. 7 Results of the micro-X-ray spectral analysis of the casting surface at the mold-metal interface: (a) surface microstructure at different magnifications; (b) elemental distribution map; (c) EDS spectra

CONCLUSION

The present study demonstrated the feasibility of using fused quartz obtained from the Aktas deposit (Kazakhstan) for the fabrication of ceramic shell molds intended for investment casting. The recommended ceramic slurry composition consisted of 70 wt.% fused quartz (particle size: 0.2-0.6 mm), 25 wt.% 15A silica sol containing 30 wt.% SiO_2, and 5 wt.% distilled water.

Compared with the reference ceramic shell system based on quartz sand, the developed fused-quartz shell molds exhibited higher gas permeability, higher residual compressive strength, and a lower coefficient of linear thermal expansion. The improved thermal stability can be attributed to the amorphous structure of fused quartz, which prevents the polymorphic transformations characteristic of crystalline quartz during heating. The combination of gas permeability and residual compressive strength demonstrated satisfactory functional performance of the developed shell system under the investigated conditions.

Experimental investment casting of the Fe–Cr–Mn–Co–Ni–Nb–Mo quasi-high-entropy alloy demonstrated that the developed shell molds retained their structural integrity during pouring and cooling. The castings showed no visible burn-on, metal penetration, or other macroscopic surface defects, and the average surface roughness was Ra = 2.65 μm. These results demonstrate satisfactory casting performance under the investigated conditions. The MXSA/EDS results provided additional evidence for the absence of measurable silicon transfer from the ceramic shell to the casting surface under the investigated casting conditions. However, the present study did not quantitatively characterise open porosity, pore-size distribution, or pore morphology; therefore, the relationship between pore structure and gas permeability requires further investigation.

Acknowledgements: This research was supported by the Science Committee of the Ministry of Science and Higher Education of the Republic of Kazakhstan under Grant AP26103843 and Program-Targeted Funding Project BR24993020.

REFERENCES

1. J. Campbell: *Complete Casting Handbook: Metal Casting Processes, Metallurgy, Techniques and Design*. 2nd ed. Oxford: Elsevier, 2015.
2. S. Jones, C. Yuan: Journal of Materials Processing Technology, 135(2-3), 2003, 258–265. https://doi.org/10.1016/S0924-0136(02)00907-X
3. S. Amira, D. Dubé, R. Tremblay: Journal of Materials Processing Technology, 211(8), 2011, 1336-1340. https://doi.org/10.1016/j.jmatprotec.2011.03.002
4. J.W. Yeh, et al.: Advanced Engineering Materials, 6(5), 2004, 299-303. https://doi.org/10.1002/adem.200300567
5. Y. Zhang, T.T. Zuo, Z. Tang, M.C. Gao, K.A. Dahmen, P.K. Liaw, Z.P. Lu: Progress in Materials Science, 61, 2014, 1-93. https://doi.org/10.1016/j.pmatsci.2013.10.001
6. D.B. Miracle, O.N. Senkov: Acta Materialia, 122, 2017, 448-511. https://doi.org/10.1016/j.actamat.2016.08.081
7. V.Y. Kulikov, A.Z. Issagulov, S.S. Kvon, Y.A. Sidorina: Metalurgija, 56(3-4), 2017, 409-411.
8. A.Z. Issagulov, S.S. Kvon, V.Y. Kulikov, A.A. Sakbossynova: Metalurgija, 53(4), 2014, 621-623.
9. W. Everhart, S. Lekakh, V. Richards, et al.: International Journal of Metalcasting, 7, 2013, 21-27. https://doi.org/10.1007/BF03355541
10. C. Mahimkar, S.N. Lekakh, V.L. Richards: Journal of Materials Engineering and Performance, 26, 2017, 2145–2153. https://doi.org/10.1007/s11665-017-2637-3
11. V. Kulikov, S. Baibekov, K. Svetlana, A. Issagulov, P. Kovalev: Acta Metallurgica Slovaca, 31(1), 2025, 16-21.https://doi.org/10.36547/ams.31.1.2128
12. P. Wisniewski, R. Sitek, A. Towarek, et al.: Materials, 13(12), 2020, 2735. https://doi.org/10.3390/ma13122735
13. A.Z. Isagulov, M.M. Akimbekova, E.P. Shcherbakova: Vestnik NAS RK, 2018(4), 2018, 112-118.
14. A.Z. Isagulov, S.S. Kvon: *Innovative Refractory Materials and Binders in Investment Casting Technology*. Karaganda: KarTU Publishing, 2015.
15. K.Z. Zhumashev, A.M. Tleuova: Trudy Universiteta, 2021(1), 2021, 29-34.
16. GOST 23409.6-78. *Molding mixtures. Method for determination of gas permeability*. Moscow: Standards Publishing, 1978.
17. ASTM C1424-15. *Standard Test Method for Monotonic Compressive Strength of Advanced Ceramics at Ambient Temperature*. West Conshohocken, PA: ASTM International, 2015.
18. J. Bidulská, R. Bidulský, M. Actis Grande, T. Kvačkaj: Materials, 12(22), 2019, 3724. https://doi.org/10.3390/ma12223724
19. J. Bidulská, R. Bidulský, M. Actis Grande, T. Kvačkaj: Archives of Metallurgy and Materials, 58(2), 2013, 371-375. https://doi.org/10.2478/amm-2013-0002
20. J. Bidulská, T. Kvačkaj, R. Bidulský, M. Actis Grande, L. Litynska-Dobrzynska, J. Dutkiewicz: Chemicke Listy, 105(S4), 2011, S471-S473.
21. S.N. Bansode, V.M. Phalle, S.S. Mantha: Transactions of the Indian Institute of Metals, 73(3), 2020, 763-773. https://doi.org/10.1007/s12666-020-01872-5
22. S.S. Kvon, V.Y. Kulikov, E.P. Melnikova: Liteishchik Rossii, 2021(6), 2021, 22-27.